The Astrophysical Journal Letters, 962:L5 (7pp), 2024 February 10 https://doi.org/10.3847/2041-8213/ad1ced

Where Did the Amaterasu Particle Come From?

Michael Unger[1,2] and Glennys R. Farrar[3]
[1] Institut für Astroteilchenphysik, Karlsruher Institut für Technologie, Karlsruhe D-76344, Germany; michael.unger@kit.edu
[2] Institutt for fysikk, Norwegian University of Science and Technology (NTNU), Trondheim, Norway
[3] Center for Cosmology and Particle Physics, Department of Physics, New York University, NY 10003, USA; gf25@nyu.edu
Received 2023 December 26; accepted 2024 January 10; published 2024 February 1

Abstract

The Telescope Array Collaboration recently reported the detection of a cosmic-ray particle, "Amaterasu," with an extremely high energy of 2.4×10^{20} eV. Here we investigate its probable charge and the locus of its production. Interpreted as a primary iron nucleus or slightly stripped fragment, the event fits well within the existing paradigm for UHECR composition and spectrum. Using the most up-to-date modeling of the Galactic magnetic field strength and structure, and taking into account uncertainties, we identify the likely volume from which it originated. We estimate a localization uncertainty on the source direction of 6.6% of 4π or 2726 deg^2. The uncertainty of magnetic deflections and the experimental energy uncertainties contribute about equally to the localization uncertainty. The maximum source distance is 8–50 Mpc, with the range reflecting the uncertainty on the energy assignment. We provide sky maps showing the localization region of the event and superimpose the location of galaxies of different types. There are no candidate sources among powerful radio galaxies. An origin in active galactic nuclei or star-forming galaxies is unlikely but cannot be completely ruled out without a more precise energy determination. The most straightforward option is that Amaterasu was created in a transient event in an otherwise undistinguished galaxy.

Unified Astronomy Thesaurus concepts: Cosmic rays (329); Ultra-high-energy cosmic radiation (1733); Milky Way magnetic fields (1057); Cosmic ray astronomy (324)

1. Introduction

Recently, the Telescope Array (TA) Collaboration reported the detection of an air shower initiated by a cosmic-ray particle with an estimated energy of $E = (2.44 \pm 0.29\,(\text{stat.})\,^{+0.51}_{-0.76}\,(\text{syst.})) \times 10^{20}$ eV (Abbasi et al. 2024). The arrival direction was (R.A., decl.) = $(255.9 \pm 0.6,\ 16.1 \pm 0.5)^\circ$ in equatorial coordinates, or $(\ell,\ b) = (36.2,\ 30.9)^\circ$ in Galactic coordinates. The TA Collaboration has named the event "Amaterasu."

At the nominal reconstructed energy, the Amaterasu event is the second most energetic particle ever recorded after the famous Fly's Eye event ($E = (3.2 \pm 0.9\,(\text{tot.})) \times 10^{20}$ eV; Bird et al. 1995). Two other extremely energetic events, within one standard deviation (total energy uncertainty) of the Amaterasu particle, have been previously reported by the Pierre Auger Collaboration (Abreu et al. 2022; Abdul Halim et al. 2023).

Our purpose in this Letter is to characterize the distance and direction of Amaterasu's source, based on its reported energy and what is known about ultra-high-energy cosmic rays (UHECRs) in general from earlier measurements of their energy spectrum and mass composition.

Assuming that the air shower was initiated by an iron nucleus (see the discussion in the next section), the nominal energy estimate of the Amaterasu event is $E_{\rm nom} = (2.12 \pm 0.25) \times 10^{20}$ eV, including the quoted corrections for resolution effects (−3%) and heavy primaries (−10%). Taking into account the 20% systematic energy scale uncertainty of the Telescope Array, a conservative energy estimate is $E_{\rm low} = (1.64 \pm 0.19) \times 10^{20}$ eV. The quoted uncertainty in both cases is due to the statistical error on the measurement of the particle density at ground level.

We approach the analysis in steps. In Section 2 we investigate the joint probability distribution in source distance and UHECR rigidity upon reaching the Galaxy, for each of the energy assignments, $E_{\rm nom}$ and $E_{\rm low}$, based on the hypothesis that the original UHECR was an iron nucleus. With this information, in Section 3 we find the probability distribution of source distance. For each rigidity value, in Section 4, we backtrack the arriving UHECR through the Galactic magnetic field (GMF) to find the source direction taking into account the uncertainties due to deflections of the coherent and turbulent GMF. Integrating over the rigidity distribution, we thereby find the localization uncertainty of the particle. Thus prepared, in Section 5 we investigate the galaxies falling in the source volume; we conclude in Section 6.

2. Particle Rigidity

Magnetic interactions of relativistic charged particles depend on their rigidity, and to good accuracy, the heavy fragments of photodissociation of nuclei have the same rigidity as the parent. This motivates the "Peters cycle" (Peters 1961) ansatz in which all nuclei except spallation protons have a common spectrum when expressed in terms of rigidity, only differing in their normalization. A standard choice is a power-law rigidity spectrum with an exponential cutoff, $\mathcal{R}^{-\gamma} \exp(-\mathcal{R}/\mathcal{R}_{\rm max})$.

An excellent description of the observed spectrum and composition of extragalactic cosmic rays at UHEs can be obtained if a maximum rigidity in the range of $10^{18.5} < \mathcal{R}_{\rm max}/{\rm V} < 10^{18.7}$ is assumed, under a wide range of assumptions including a pure Peters cycle or modified scenarios with photonuclear or hadronic interactions in the source environment (see, e.g., Aab et al. 2017; Unger et al. 2015; Muzio et al. 2022, respectively). Given $\mathcal{R}_{\rm max}$ in this range, the accelerators are powerful enough to produce an

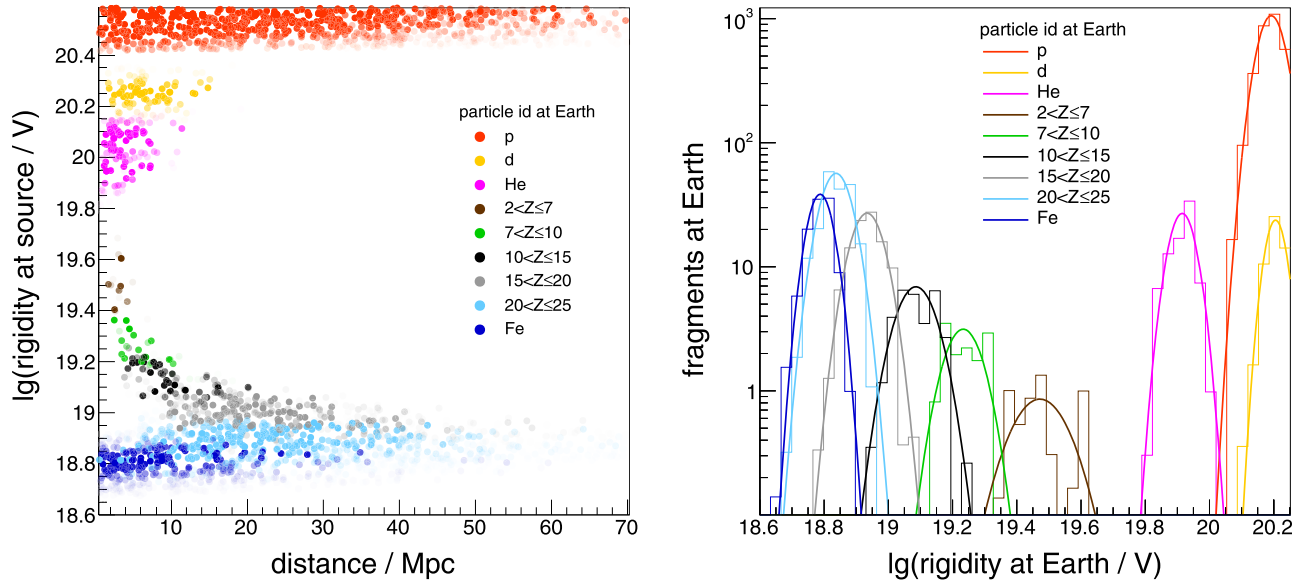

Figure 1. Simulation of the propagation through extragalactic photon fields of a UHECR, which originates as $^{56}_{26}$Fe, with a uniform distance distribution and an E^{-1} energy spectrum (no cutoff) at the source. *Left:* injected rigidity vs. source distance. Each point denotes a fragment of an iron nucleus that reaches Earth with an energy similar to the one of the Amaterasu particle. The transparency of each point encodes the likelihood the energy is reconstructed to be $E_{\rm low}$, w_E. The particle type of the fragments arriving at Earth are shown as colors. *Right:* rigidity distribution of the fragments arriving at Earth. Lines are Gaussian fits to the histograms. Histogram entries are weighted according to their deviation from the measured energy of the TA event, w_E. These plots are for the low energy scale for the Amaterasu particle.

Amaterasu particle in the tail of the rigidity spectrum if it is an iron nucleus ($Z = 26$), since, e.g., $\exp(-E_{\rm nom}/(26 \times 10^{18.7}{\rm V})) = 0.15$.[4]

For the air shower detected by TA to have been initiated by a proton, some entirely new acceleration mechanism must be invoked. On the other hand, since the event fits well to the UHE end of the energy spectrum reported by Kim et al. (2023) and since the TA flux at these energies is well described by iron nuclei (see Figure 8 in Unger et al. 2015), the minimal assumption on the nature of the particle is that it is an iron nucleus from the bulk of the cosmic-ray flux at UHE. Therefore, we focus on iron nuclei injected at the source as the most plausible origin of Amaterasu.

We next constrain the distance and rigidity of the initial iron cosmic ray, which evolved into the observed Amaterasu particle detected at Earth. The source distance will limit what extragalactic objects are candidates to be the source, and the rigidity is needed to account for deflection in the GMF to backtrack to the source direction. To determine the distance and rigidity distributions, we simulate the propagation of a UHECR, which originates as an iron nucleus, through the cosmic microwave background radiation and the extragalactic background light (Gilmore et al. 2012) with CRPROPA3 (Alves Batista et al. 2016). We generated events uniformly in distance and with an energy spectrum $\propto E^{-1}$—the approximate spectral index of UHECRs at the source, as deduced from the combined spectrum and composition data.

The left panel of Figure 1 shows a scatterplot of the source distance and initial rigidity (=initial energy/26) of events arriving at Earth with an energy of $E_\oplus = E_{\rm low}$ (the corresponding plots for $E_{\rm nom}$ look similar, but with a reduced range in distance). The opacity of the points is proportional to

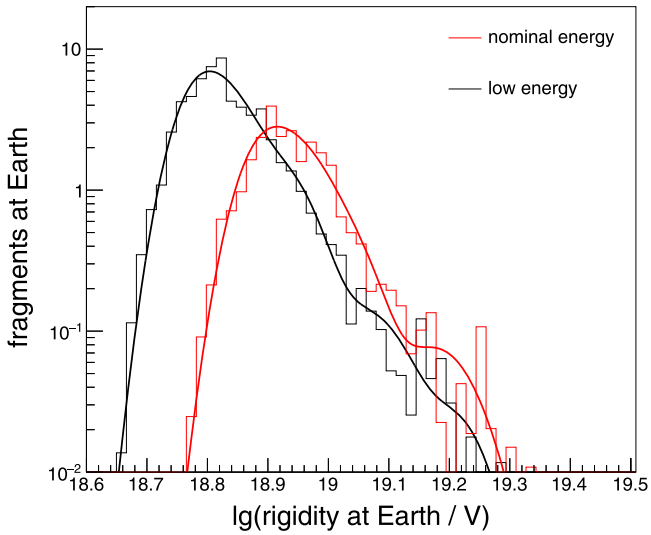

Figure 2. Distribution of the event rigidity at Earth, compatible with the detected energy at the nominal and low energy scales.

$w_E \equiv [b]\exp[-\frac{1}{2}((E_\oplus - \widehat{E})/\hat{\sigma})^2]$, i.e., proportional to the Gaussian probability to reconstruct $\widehat{E}$ given the simulated energy $E_\oplus$ at Earth, and the measurement uncertainty $\hat{\sigma}$. The right panel of Figure 1 is a projection in source distance of the left panel, displaying the histogram of rigidities for each mass group.

Including a second weight $w_{\mathcal{R}} \equiv \exp(-\mathcal{R}/\mathcal{R}_{\rm max})$ to model the injected rigidity distribution mostly suppresses the tail of low-mass fragments, given a specified observed energy. The fit of TA data with iron primaries in Unger et al. (2015) suggests $\mathcal{R}_{\rm max} = 10^{18.7}$ V for the nominal energy scale; for the low energy scale we use $\mathcal{R}_{\rm max} = 10^{18.6}$ V. Summing over species, Figure 2 shows the distribution of the logarithm of the rigidity of the observed events, weighted with $w_E \cdot w_{\mathcal{R}}$, for the two

[4] A subdominant population of more powerful accelerators might exist with a best-fit maximum rigidity in the range of $10^{19.1} < \mathcal{R}^{\rm sub}_{\rm max}/{\rm V} < 10^{19.5}$ (Muzio et al. 2019; Ehlert et al. 2023; Halim et al. 2023). However, Amaterasu has too high an energy for it to be identified as a part of this subdominant proton population.

energy scales. The fraction by charge group ($7 < Z \leqslant 10$, $10 < Z \leqslant 15$, $15 < Z \leqslant 20$, $20 < Z \leqslant 25$, Fe) of detected UHECR, for iron injected at the source with a maximum rigidity of $\lg \mathcal{R}_{\rm max}/{\rm V} = 18.7$ and 18.6, compatible with the Amaterasu particle at the nominal and low energy scale is (0, 2.4, 13.4, 50.7, 33.4)% and (0.4, 2.4, 15.6, 48.1, 33.3)%, respectively. Their mean and standard deviations are

$$\lg(\mathcal{R}/{\rm V}) = 18.94 \pm 0.07 \quad \text{and} \quad 18.83 \pm 0.07 \qquad (1)$$

for the nominal and low energy scales, respectively.

3. Propagation Distance

The discussion of the previous section was for a fixed observed energy value, $E_{\rm nom}$ or $E_{\rm low}$, but the experimental statistical uncertainty needs to be taken into account. Figure 3 shows a histogram of the propagation distance as a function of the UHECR energy at Earth, for a maximum rigidity of $10^{18.6}$ V . The vertical lines mark the central and $\pm 1\sigma_{\rm stat}$ energy values. One sees that the energy scale uncertainty is presently so great as to lead to a factor 2.5 uncertainty on the source distance.

We define the approximate edge of the source volume as the distance, $D_{0.1}$, at which the flux is attenuated by a factor 10 relative to the case with no photointeraction energy losses. This distance is $D_{0.1} = 12.6^{+7.9}_{-4.3}$ Mpc and $33.5^{+16.3}_{-10.9}$ Mpc for the nominal and low energy scale, respectively. The uncertainties originate from the 1σ statistical uncertainty on the particle energy; there is negligble sensitivity to the $\mathcal{R}_{\rm max}$ choice. Thus, taking the lower and upper 1σ bounds of these uncertainties, the outer radius of the volume of possible sources is between 8 and 50 Mpc, for a factor of 240 uncertainty in the volume containing the source.[5]

4. Arrival Direction

We backtracked Amaterasu through the GMF to identify the domain of highest source likelihood using the ensemble of eight models of the coherent GMF from Unger & Farrar (2023) that are compatible with the existing astrophysical tracers of the magnetic field of the Milky Way and encompass the range of uncertainty in the GMF. We generate realizations of the random field with the power spectrum taken to be that of a turbulent cascade (Kolmogorov 1941) using the method of Giacalone & Jokipii (1999). We adopt 100 pc for the outer scale of the turbulence as expected for supernova-driven turbulence and produce a unit-norm random field from a superposition of 300 random waves spaced logarithmically between 0.1 and 100 pc, corresponding to a coherence length of 20 pc. This unit-norm random field is then weighted by the rms field strength of the Planck-tune of the JF12 random field (Jansson & Farrar 2012b; Adam et al. 2016).

Figure 4 shows, in Galactic coordinates, the ensemble of backtracked events for the nominal (left column) and low energy (right column) median rigidity assignments for 1000 events with a $\approx 0^\circ.5$ Gaussian uncertainty in the measured (R. A.,decl.) angles of the arrival direction. The first row shows the result for a unique rigidity and single realization of the random field. The next row shows the superposition of results for 35 different realizations of the random field. Finally, the bottom row shows the source direction distribution summing over the uncertainty in the rigidity distribution shown in Figure 2. In each case, the colored lines show the 68% convex hull contours (McDermott & Lin 2007) of the backtracking results for each of the eight GMF model variations. The open crosses in the top row show the backtracked central arrival directions for the JF12 coherent field.

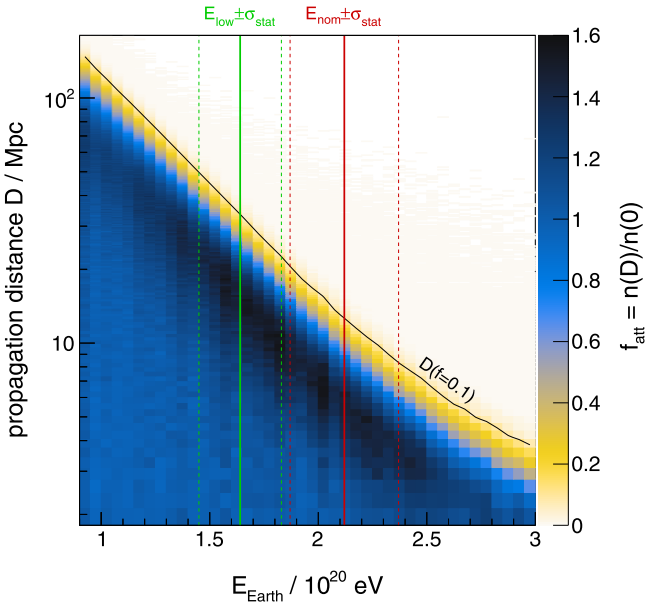

Figure 3. Propagation distances of cosmic rays arriving at Earth, in each bin of energy as given on the x-axis of the plot, for iron injected with an $\mathcal{R}_{\rm max} = 10^{18.6}$V energy spectrum. The normalized number of cosmic rays per distance bin is indicated by the color scale. The nominal and low energy (thick central lines) of the Amaterasu particle, with the one standard deviation of the statistical reconstruction uncertainty (dashed lines), are superimposed. The distance, $D_{0.1}$, at which the relative number of arriving fragments drops below 10% of the value at zero distance is shown as a black line.

The meaning of the gray scale is somewhat nontrivial because we do not know a priori which of the eight coherent field models of Unger & Farrar (2023) is closest to the truth. An arrival direction should not be deemed unlikely because it is far from the bulk of the models if it is compatible with the (unknown to us) best model. Therefore, we proceed as follows. The density of backtracked particles is displayed with gray scales on an $N_{\rm side} = 32$ HEALPIX grid. Here we first collect the density maps of each model j separately and normalize the density in each pixel i to the maximum density value for the given map, $\rho_{ij} = N_{ij}/N_{{\rm max},j}$. Here N_{ij} is the number of backtracked particles in pixel i of the skymap of GMF model j and $N_{{\rm max},j} = \max_{1 \leqslant j \leqslant n} N_{ij}$ with the number of pixels n. The union of the density of all models is then

$$\rho_i = \max_{1 \leqslant j \leqslant 8} \rho_{ij}, \qquad (2)$$

i.e., for a particular direction i of the sky, ρ_i is the density of the closest GMF model variation.

The resulting source direction uncertainty is a compounded combination of the uncertainty in arrival direction; the uncertainty in the coherent field reflected in the model-to-model differences between the eight different GMF models, which is amplified due to random fields on top of the coherent

[5] Note that our definition of the horizon differs from that used in Kuznetsov (2023), where the horizon is defined to be the distance within which 95% of the integral flux above a specified energy originated, assuming a uniform source distribution and an $E^{-1.89}$ spectrum without cutoff. Here we are interested in the probability distribution in distance of the individual source responsible for this particular event, therefore in this context our definition is more suitable.

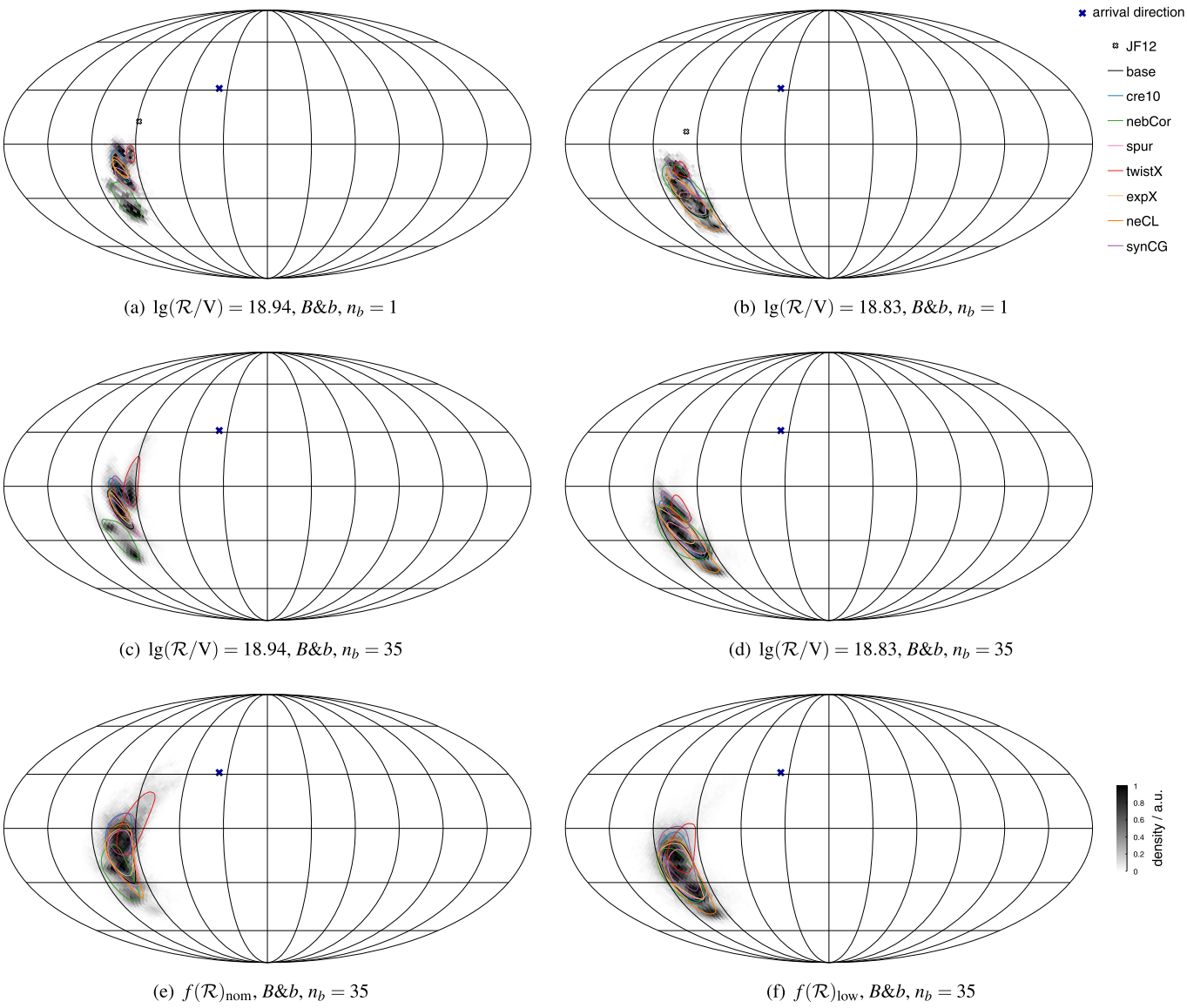

(a) $\lg(\mathcal{R}/\mathrm{V}) = 18.94$, $B\&b$, $n_b = 1$

(b) $\lg(\mathcal{R}/\mathrm{V}) = 18.83$, $B\&b$, $n_b = 1$

(c) $\lg(\mathcal{R}/\mathrm{V}) = 18.94$, $B\&b$, $n_b = 35$

(d) $\lg(\mathcal{R}/\mathrm{V}) = 18.83$, $B\&b$, $n_b = 35$

(e) $f(\mathcal{R})_{\mathrm{nom}}$, $B\&b$, $n_b = 35$

(f) $f(\mathcal{R})_{\mathrm{low}}$, $B\&b$, $n_b = 35$

Figure 4. Density of arrival directions backtracked to the edge of the galaxy for eight GMF model variations from Unger & Farrar (2023); results for the nominal and low energy scales are shown in the left and right columns, respectively. We use Galactic coordinates with the Galactic center at the origin and the longitude increasing toward the left. The measured arrival direction of the Amaterasu particle is shown as a blue cross. For reference, the backtracked direction in the coherent field of Jansson & Farrar (2012a) is shown as an open cross in the top row. For all panels, the magnetic field is a superposition of a regular (B) and a turbulent (b) component. The top row shows one particular realization of the turbulent field ($n_b = 1$). The middle and bottom rows show a superposition of the results for 35 different realizations of b ($n_b = 35$). The top and middle panels were calculated at a fixed rigidity (the mean values given in Equation (1)), while the bottom row is for the full distribution of rigidities (see Figure 2). The colored contours show the 68% confidence level convex hulls for each GMF model.

one; the "Galactic variance" from different realizations of the random field; and the uncertainty in the rigidity, which is responsible for the difference between the middle and last rows. Note that the overall coherent deflection is larger than the uncertainty in the deflections.

We define the source localization region to be the area on the sky in which the density defined in Equation (2) is larger than 0.05. For both energy scales, this results in a solid angle of 3.5% of 4π for the maps in the middle panel of Figure 4, i.e., when including the uncertainties originating from the magnetic field (coherent models, random field, and Galactic variance). Including the rigidity distribution (lower panel of Figure 4) yields a larger value of 5.5% and 4.6% for the nominal and low energy scales, respectively. Finally, the full uncertainty, including the energy of Amaterasu, is conservatively estimated by using the maximum of the two density maps of Figures 4(e) and (f). This yields a localization uncertainty Ω_{loc} of 6.6% of 4π or 2726 deg^2. About half of this uncertainty can be attributed to the GMF and the other half originates from the energy uncertainty (statistical and systematic).[6]

[6] The typical standard deviation of the deflection angle after traversing a distance D the turbulent extragalactic magnetic field (EGMF) of strength B with coherence length λ is $[b]\theta_{\mathrm{eg}} = 2.5^\circ \sqrt{D/l}\ (\lambda/1\ \mathrm{Mpc})(B/1\ \mathrm{nG})/(\mathcal{R}/10^{19}\ \mathrm{V})$ (Waxman & Miralda-Escude 1996). The contribution to the estimated localization uncertainty can be neglected if $\theta_{\mathrm{eg}} < \theta_{\mathrm{loc}}$ where $\theta_{\mathrm{loc}} = \arccos(1 - \Omega_{\mathrm{loc}}/2\pi) = 28^\circ$. Assuming a conservative value of $\lambda = 1$ Mpc and the upper limit on the EGMF of $B \leqslant 1\ nG$ (Durrer & Neronov 2013; Pshirkov et al. 2016) yields $\theta_{\mathrm{eg}} \leqslant 21^\circ$ and $\theta_{\mathrm{eg}} \leqslant 10^\circ$ for the propagation horizon $D_{0.1}$ and rigidity corresponding to E_{low} and E_{nom}, respectively. The total localization angle $[b]\theta_{\mathrm{tot}} = \sqrt{\theta_{\mathrm{loc}}^2 + \theta_{\mathrm{eg}}^2}$ is thus at most 25% larger than θ_{loc}, i.e., the localization is robust concerning the EGMF.

5. Comparison to Galaxy Catalogs

As a preliminary step to identifying astrophysical objects that could be responsible for accelerating Amaterasu, we identify objects in three catalogs used by the Pierre Auger Collaboration (Abdul Halim et al. 2023) that fall within the localization volume. These catalogs are (a) the flux-limited Two Micron All Sky Survey (2MASS; Huchra et al. 2012) cross-matched with the HyperLEDA distance database (Makarov et al. 2014), (b) the flux-limited Swift-BAT 105 month catalog of active galactic nuclei (AGNs) observed in hard X-rays (Oh et al. 2018), and (c) a sample of nearby starburst galaxies (SBGs) from Lunardini et al. (2019). In addition, we investigate (d) radio galaxies (RGs) from the volume-limited catalog of van Velzen et al. (2012). Not all RGs pass the luminosity criterion (Waxman 1995; Blandford 2000; Farrar & Gruzinov 2009) to be viable candidates for accelerators up to the rigidity of the Amaterasu particle, and we therefore use only the subset identified as satisfying that requirement by Matthews et al. (2018). For completeness, we also included galaxies from the "Local Volume catalog" of Karachentsev et al. (2018), a volume-limited sample of galaxies up to a distance of 11 Mpc.

The position of each of these galaxies within a distance of $D = 125$ Mpc is displayed in Figure 5(a). The galaxies from the 2MASS and Swift-BAT catalogs are shown as gray and red points, respectively. RGs and SBGs with flux greater than 5% that of the brightest local source of their type, i.e., Cen A (RGs) and M82 (SBGs), are shown with black and green symbols whose area is proportional to the 1.1 and 1.4 GHz radio flux, respectively. (The 1.4 GHz radio flux was taken as a proxy for UHECR production by Abdul Halim et al. 2023.) Galaxies with a flux greater than 10% of the brightest local source are labeled with names. Galaxies from the Local Volume catalog are shown in orange and the four galaxies that dominate the local volume in terms of stellar mass divided by distance-squared are shown with labels and large symbols. The subsequent panels zoom into the localization region of the Amaterasu source, starting $2\sigma_{\rm stat}$ below $E_{\rm low}$ and increasing to $E_{\rm nom}$, showing the correspondingly shrinking horizon as a function of the actual energy of the event.

We thus have identified, for each Amaterasu energy assignment, a very conservative (maximal) source volume—the angular locus and maximum depth of the source—taking into account the uncertainty in GMF and rigidity. For each energy assignment, we can ask what candidate sources fall within the volume. A source class that is entirely absent from the volume cannot be responsible for Amaterasu at that energy. If there are some candidates then we assess the plausibility of that class by comparing its flux proxy for the sources inside the source localization to the total flux proxy within the horizon. Since we are discussing a single event, the flux ratio gives the probability that, under the hypothesis that the UHECR flux follows the proxy, the Amaterasu source happens to fall in that particular region of the sky.

We start with RGs, long a favorite source candidate. No RGs satisfying the luminosity criteria lie within the localization volume unless Amaterasu's energy is at least $2\sigma_{\rm syst.}$ lower than $E_{\rm low}$; then, three galaxies appear (NGC0262, NGC0315, and NGC7626). However, the three galaxies contribute only 0.2% of the total flux, from which alone one could exclude an origin of Amaterasu in RGs at the 3σ level. Taking into account that in addition we required a 2σ downward fluctuation of $E_{\rm low}$ to increase the horizon, makes this source hypothesis very unlikely.

Ordinary Swift-BAT AGNs are another candidate. A total of 6 out of 130 of them with $D \leqslant 72$ Mpc are within the localization shown in Figure 5(b) for energy $E_{\rm low} - 2\sigma_{\rm stat.}$, but none for a higher energy assignment. These six galaxies contribute 1% to the total X-ray flux from Swift-BAT galaxies within the 72 Mpc horizon at this energy assignment. Similarly to the case of RGs, the combination of having to go to such a low energy assignment in order to have any Swift-BAT AGN candidates, and the low combined flux of the candidate sources relative to those within the horizon but in other directions, is in strong tension with X-ray AGNs being the source of Amaterasu.

The Amaterasu event is also in tension with the proposal that UHECR sources are found in SBGs. No SBG falls within the source direction domain for the three low energy assignments. Only at the nominal energy is the angular deflection small enough that the starburst NGC6946 lies just at the edge of the angular localization region using the "twistX" GMF variant (see Figure 4(e)) as can be seen in Figure 5(e). (We recall that at the boundary, the weight in the source direction distribution is 0.05 times its peak value for the most favorable GMF model, so some directional tension remains even with the twistX GMF model.) The 1.4 GHz radio flux of this galaxy, used as UHECR flux proxy in Aab et al. (2018) and Abdul Halim et al. (2023), is about 20% of the flux of the brightest SBGs of the catalog, M82 and NGC4945 (a candidate for causing the "Auger hotspot"), and contributes 3% to the summed flux of all sources within the horizon at this energy, $D_{0.1} = 10$ Mpc.

For reference, the contribution of the K-band flux of 2MASS galaxies within the localization volume is at the 1%–2% level relative to the all-sky flux of 2MASS galaxies within the horizon for all four energies displayed. Given that the localization area is of order 6.6% of the sky, the relative paucity of flux reflects the general underdensity of galaxies in the source volume, already noted by TA. As a matter of information, but only relevant for the nominal energy scenario, the underdensity disappears when using galaxies in the Local Volume catalog. In this region, the source volume "flux" (stellar mass per distance-squared) is dominated by M31 (Andromeda) and is 6% of the total.

6. Summary and Conclusions

We have studied the likely composition and origin of the UHECR event Amaterasu, recently reported by the Telescope Array Collaboration (Abbasi et al. 2024). We find that Amaterasu fits nicely into the existing accumulated understanding of UHECR composition and spectrum if it is an iron nucleus or fragment thereof. By contrast, identifying Amaterasu as a proton or light nucleus would demand that it be produced by an entirely new source class. Adopting, therefore, the minimalist interpretation of an intermediate or heavy nucleus and following the prescription for the corresponding energy assignment given by Abbasi et al. (2024), we considered two energies for the particle: the nominal energy of $E_{\rm nom} = (2.12 \pm 0.25) \times 10^{20}$ eV and $1\sigma_{\rm syst.}$ lower $E_{\rm low} = (1.64 \pm 0.19) \times 10^{20}$ eV. Detecting an event in this energy range is natural—even expected—given accumulated exposure of TA, based on extrapolating the spectrum already reported by TA; see Figure 4 of Kim et al. (2023).

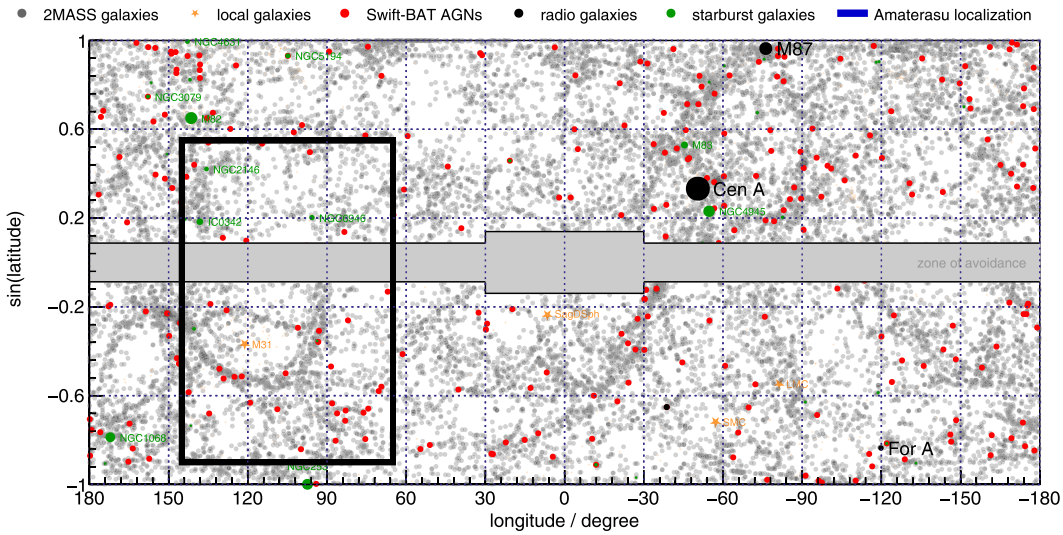

(a) Distribution of galaxies up to $D = 125$ Mpc. The area zoomed in the lower panels (b)-(e) is indicated by a black rectangle.

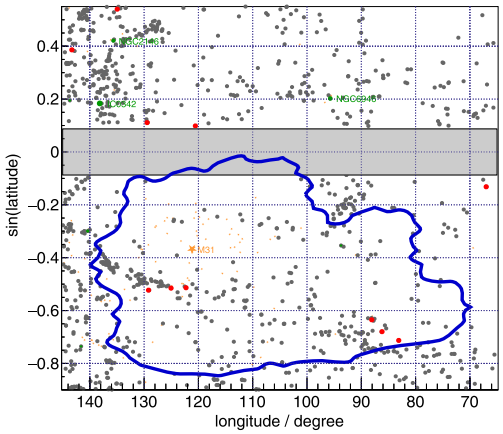

(b) $E_{\rm low} - 2\,\sigma$, $D_{0.1} = 72$ Mpc

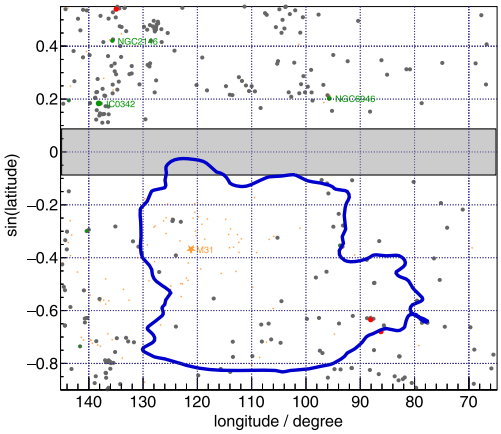

(c) $E_{\rm low} - 1\,\sigma$, $D_{0.1} = 42$ Mpc

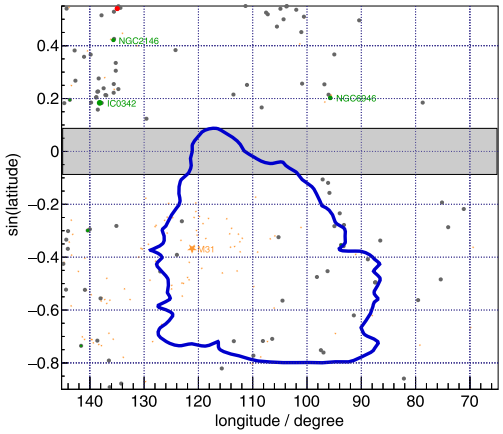

(d) $E_{\rm low}$, $D_{0.1} = 25$ Mpc

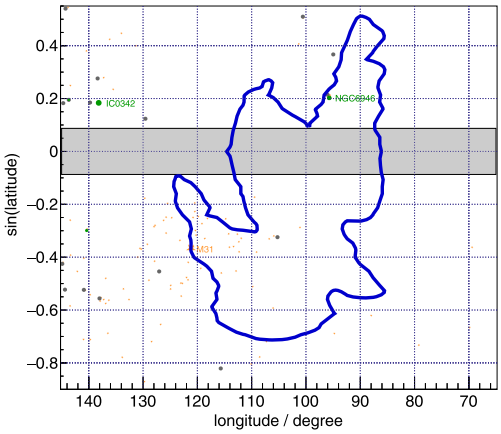

(e) $E_{\rm nom}$, $D_{0.1} = 10$ Mpc

Figure 5. Galaxies within various distances for comparison to the source localization domain in Galactic coordinates. The top panel shows all galaxies up to a distance of 150 Mpc, the other plots include galaxies up to the attenuation horizon, $D_{0.1}$ depending on the rigidities corresponding to the particle energy assumed, see Equation (1) particle energy indicated. Contours of the distribution of backtracked particles are shown in blue at $\rho = 0.05$, see Equation (2). The different colors denote galaxies from the 2MASS survey (gray), galaxies in the local volume, $D < 11$ Mpc (orange), AGN (red), RGs (black), and SBGs (green).

Taking into account interactions with the extragalactic background light en route to Earth, and assuming that Amaterasu originated as an iron nucleus, we conclude it was produced by a source whose distance is within 8 Mpc, or up to 50 Mpc, depending on its energy. About one-third of the time, the original nucleus survives intact, and about half the time, its charge upon reaching Earth is in the range of 20–25; only a few percent of cases arrive with $Z \leqslant 15$.

We backtracked Amaterasu through the GMF to identify the domain of the highest source likelihood. Altogether we used 8×35 different GMF realizations, based on the eight coherent GMF models in the UF23 suite (Unger & Farrar 2023), which in their ensemble encompass the range of uncertainty in the large-scale Galactic field. Added to each of the coherent GMF models was one of 35 different random field realizations, whose field strength is given by the Planck-tune of the JF12 random field (Adam et al. 2016). Taking the union of field models and Amaterasu rigidities, we obtain a conservative angular locus for the source for each energy assignment. Combined with the source distance constraint, we identify the most probable source volume for each Amaterasu energy assignment.

Finally, interrogating catalogs of sufficiently powerful RGs, Swift-BAT AGNs, SBGs, and generic galaxies, we assess which of these galaxy types can have produced Amaterasu. We find that none of the "usual suspects" among candidate nontransient UHECR accelerators provides a comfortable explanation. There are simply no RGs of sufficient power within the localization volume, unless the energy is $2\sigma_{\rm stat.}$ below $E_{\rm low}$. Moreover, even though the horizon is so large in this case that a few RG candidates appear in the source volume, their total UHECR flux proxy is only a fraction of a percent of that of the rest of the sky. Similarly, only for this lowest energy assignment are there any candidate Swift-BAT AGNs, and those are also deprecated by having a small total flux proxy relative to Swift-BAT AGNs in the rest of the sky.

A third popular candidate to host UHECR accelerators is SGBs. SBGs are of primary interest because long GRBs result from the collapse of massive young stars, hence their rate is enhanced in SGBs. However, SBGs are also deprecated as a possible source of Amaterasu by this analysis. Only for the highest energy assignment is there an SBG (barely) in the localization domain for a single GMF model, and its flux proxy is only 5% that of SBGs outside the localization region.

The most straightforward explanation for Amaterasu seems to be that it was produced by a transient in an otherwise ordinary galaxy. Several types of transients found in ordinary galaxies merit consideration, including tidal disruption events (Farrar & Gruzinov 2009), young magnetars (Blasi et al. 2000; Arons 2003), and potentially jet formation in neutron star–black hole (or possibly binary neutron star) mergers. A similar conclusion was reached by Fitoussi et al. (2020), who attribute the nominally 320 EeV "Fly's Eye" event to an iron nucleus from a stellar transient.[7]

Our work underscores the power of a single well-measured, high-energy event, combined with the ability to measure or estimate the composition on theoretical grounds, for restricting the possible sources of individual high-energy UHECRs. Future analysis of the TA energy calibration may enable Amaterasu's energy to be more accurately bracketed, which would increase the value of this single event even further. For instance, if the energy assignment is reduced sufficiently below the current nominal value, SBGs would be eliminated as a possible source, while if the lower bound on the energy can be shown to be clearly above ≈130 EeV, RGs and Swift-BAT AGNs could be excluded.

[7] Fitoussi et al. (2020) ignored the coherent deflections of the Fly's Eye event, detected at $(\ell, b) = (163.4, 9.6)°$. We checked that approximation, finding an average backtracked extragalactic arrival direction of $(165 \pm 3, 14.7 \pm 8.5)°$, assuming a rigidity of $\mathcal{R} = 7.3$ EV, where the uncertainties give the maximum range of the predictions from the eight GMF models of Unger & Farrar (2023).

Acknowledgments

We would like to thank Luis Anchordoqui, Ralph Engel, Toshihiro Fujii, Mikhail Kuznetsov, and Foteini Oikonomou for useful discussions. The research of GRF has been supported by the National Science Foundation grant NSF-PHY-2013199.

ORCID iDs

Michael Unger https://orcid.org/0000-0002-7651-0272
Glennys R. Farrar https://orcid.org/0000-0003-2417-5975

References

Aab, A., Abreu, P., Pierre Auger Collaboration, et al. 2017, JCAP, 04, 038
Aab, A., Abreu, P., Pierre Auger Collaboration, et al. 2018, ApJL, 853, L29
Abbasi, R., Allen, M. G., Telescope Array Collaboration, et al. 2024, Sci, 382, 903
Abdul Halim, A., Abreu, P., Pierre Auger Collaboration, et al. 2023, ApJS, 264, 50
Abreu, P., Aglietta, M., Pierre Auger Collaboration, et al. 2022, ApJ, 935, 170
Adam, R., Ade, P. A. R., Pierre Auger Collaboration, et al. 2016, A&A, 596, A103
Alves Batista, R., Dundovic, A., Erdmann, M., et al. 2016, JCAP, 05, 038
Arons, J. 2003, ApJ, 589, 871
Bird, D. J., Corbato, S. C., Fly's Eye Collaboration, et al. 1995, ApJ, 441, 144
Blandford, R. D. 2000, PhST, 85, 191
Blasi, P., Epstein, R. I., & Olinto, A. V. 2000, ApJL, 533, L123
Durrer, R., & Neronov, A. 2013, A&ARv, 21, 62
Ehlert, D., van Vliet, A., Oikonomou, F., & Winter, W. 2023, arXiv:2304.07321
Farrar, G. R., & Gruzinov, A. 2009, ApJ, 693, 329
Fitoussi, T., Medina-Tanco, G., & D'Olivo, J.-C. 2020, JCAP, 01, 042
Giacalone, J., & Jokipii, J. R. 1999, ApJ, 520, 204
Gilmore, R. C., Somerville, R. S., Primack, J. R., & Dominguez, A. 2012, MNRAS, 422, 3189
Halim, A. A., Abreu, P., Aglietta, M., et al. 2023, JCAP, 05, 024
Huchra, J. P., Macri, L. M., Masters, K. L., et al. 2012, ApJS, 199, 26
Jansson, R., & Farrar, G. R. 2012a, ApJ, 757, 14
Jansson, R., & Farrar, G. R. 2012b, ApJL, 761, L11
Karachentsev, I. D., Kaisina, E. I., & Makarov, D. I. 2018, MNRAS, 479, 4136
Kim, J., Ivanov, D., Jui, C., & Thomson, G. 2023, EPJ Web Conf., 283, 02005
Kolmogorov, A. 1941, DoSSR, 30, 301
Kuznetsov, M. Y. 2023, arXiv:2311.14628
Lunardini, C., Vance, G. S., Emig, K. L., & Windhorst, R. A. 2019, JCAP, 2019, 073
Makarov, D., Prugniel, P., Terekhova, N., Courtois, H., & Vauglin, I. 2014, A&A, 570, A13
Matthews, J. H., Bell, A. R., Blundell, K. M., & Araudo, A. T. 2018, MNRAS, 479, L76
McDermott, J. P., & Lin, D. K. J. 2007, IIE Trans., 39, 581
Muzio, M. S., Farrar, G. R., & Unger, M. 2022, PhRvD, 105, 023022
Muzio, M. S., Unger, M., & Farrar, G. R. 2019, PhRvD, 100, 103008
Oh, K., Koss, M., Markwardt, C. B., et al. 2018, ApJS, 235, 4
Peters, B. 1961, NCim, 22, 800
Pshirkov, M. S., Tinyakov, P. G., & Urban, F. R. 2016, PhRvL, 116, 191302
Unger, M., & Farrar, G. 2023, arXiv:2311.12120
Unger, M., Farrar, G. R., & Anchordoqui, L. A. 2015, PhRvD, 92, 123001
van Velzen, S., Falcke, H., Schellart, P., Nierstenhoefer, N., & Kampert, K.-H. 2012, A&A, 544, A18
Waxman, E. 1995, PhRvL, 75, 386
Waxman, E., & Miralda-Escude, J. 1996, ApJL, 472, L89